Molten Wood's-Metal Flow in a Cylindrical Bath Agitated by Cold Bottom-Gas Injection

MANABU IGUCHI and HIROHIKO TOKUNAGA

Investigation was made of the heat-transfer effect on the motions of cold bubbles and molten metal in a bottom-blown bath. The heat transfer between the bubbles and the molten metal finished at an axial position near the nozzle exit. The bubble and liquid-flow characteristics measured above this position were in good agreement with those in a bath agitated by isothermal gas injection of the same mass flow rate. A simplified mathematical model was proposed to describe the two characteristics. The experimental results of gas holdup and mean liquid-flow velocity were satisfactorily predicted by it. The accuracy of the prediction became higher as the distance from the nozzle exit increased, due to disintegration of bubbles.

I. INTRODUCTION

MANY mathematical and physical model investigations have been carried out to clarify the behavior of bubbles and the velocity of molten metal flow in a cylindrical bath agitated by bottom-gas injection.[1–6] Most of them are concerned with isothermal gas injection. Namely, the temperature of the injected gas is the same as that of the liquid in the bath, and, hence, heat transfer does not take place between the two fluids. On the other hand, information on the motion of bubbles and liquid induced by nonisothermal gas injection is very limited,[7–10] although such injection is the case in real steelmaking processes.

The main objectives of this study are to measure the behavior of bubbles and molten Wood's-metal flow in a bath agitated by cold helium gas injection and to demonstrate the adequacy of a mathematical model proposed by the authors. The gas holdup and mean bubble-rising velocity were measured with a two-needle electroresistivity probe,[11] and the mean velocity of molten Wood's-metal flow was measured with a magnet probe.[12,13] The model was originally proposed for isothermal gas injection.[14] It will be modified here to be capable of taking the heat-transfer effect into consideration.

II. HEAT TRANSFER BETWEEN BUBBLE AND LIQUID IN BUBBLING JET

In a previous study,[7] a method was proposed to measure the heat transfer between bubbles and liquid in a bottom-blown bath. The air or helium gas was cooled to 163 K(-110 °C) and then injected into a water bath of room temperature. The motions of rising bubbles thus generated were recorded with a high-speed video camera, and the surface area of each bubble was determined using the video images. The temperature in each bubble was measured with a microthermocouple. On the basis of these data, the overall heat-transfer coefficient between the bubble and the surrounding water (U_m) was determined. The visualization technique is not applicable to opaque liquids such as molten metals. An electroresistivity probe, therefore, was selected to measure the bubble diameter in the molten Wood's-metal bath.[8] However, it is difficult to strictly separate the gas-side and liquid-side heat-transfer coefficients. This situation does not lead a problem in practical applications.

The experimentally measured values of the overall heat-transfer coefficient for air-water, helium-water, and nitrogen–molten Wood's-metal systems were found to be satisfactorily predicted by the following empirical equations:[7,8]

$$\mathrm{Nu}_{mp} = 1.1\,(\mathrm{Pe}/(1+\kappa))^{0.7} \quad [1]$$

$$\mathrm{Nu}_{mp} = U_m \bar{d}_B/\lambda_g \quad [2]$$

$$\mathrm{Re}_B = \bar{u}_B \bar{d}_B/\nu_L \quad [3]$$

where Nu_{mp} is the Nusselt number, Pe (equal to $\mathrm{Re}_B\mathrm{Pr}_g$) is the Peclet number, κ is the dynamic viscosity ratio of liquid to gas, Re_B is the bubble Reynolds number, Pr_g is the Prandtl number of gas, $\bar{u}_B$ is the mean bubble-rising velocity, $\bar{d}_B$ is the volume-equivalent bubble diameter, and ν_L is the kinematic viscosity of liquid. This equation is selected to estimate the overall heat - transfer coefficient in the mathematical modeling.

It should be noted that U_m is nearly equal to the gas-side heat-transfer coefficient (h_g):

$$U_m \cong h_g \quad [4]$$

Equation [4] means that the heat transfer between gas and liquid is mainly controlled by the gas-side heat transfer.

Bubbles generated at the nozzle exit expand, rising in the bath due to heat exchange with the liquid around them and due to a change in the static pressure. Convection and radiation heat transfer govern the bubble expansion due to the heat exchange. The expansion can be described by the following equations:[7,15,16]

$$c_g\rho_g V_g\, d\theta_g/dt = U_m A(\theta_L - \theta_g) + \sigma(\theta_L^4 - \theta_g^4)A/(1/\varepsilon_L + 1/\varepsilon_g - 1) \quad [5]$$

$$U_m = 1.1\,\lambda_g\,(\mathrm{Pe}/(1+\kappa))^{0.7}/\bar{d}_B \quad [6]$$

$$V_g = \pi \bar{d}_B^{\,3}/6 \quad [7]$$

MANABU IGUCHI, Professor, is with the Division of Materials Science and Engineering, Graduate School of Engineering, Hokkaido University, Sapporo, 060-8628 Japan. Contact e-mail: gaku@eng.hokudai.ac.jp HIROHIKO TOKUNAGA, Manager, is with Hitachi Zosen Corp., Osaka, 559-8559 Japan.

Manuscript submitted January 15, 2002.

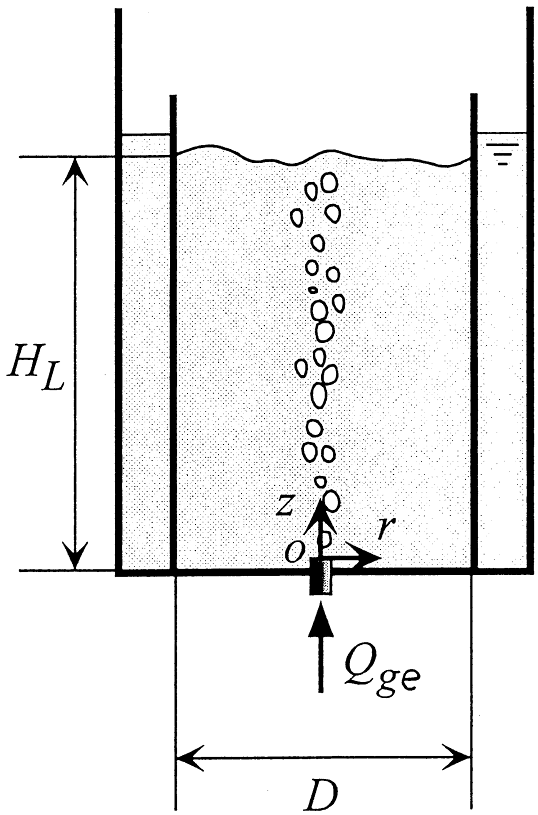

Fig. 1—Coordinate system for the experimental arrangement.

$$V_g = V_{ge} \text{ at } z = 0 \quad [8]$$

where c_g is the specific heat of gas, V_g is the bubble volume, t is time, A is the interfacial area between the bubble and liquid, σ is the Stefan–Boltzmann constant, ε is the emissivity, and z is the axial distance measured from the nozzle exit. The subscripts L, g, and e denote the liquid, gas, and nozzle exit, respectively. As U_m involves the bubble diameter and the mean bubble-rising velocity, the mean bubble temperature (θ_g) should be solved together with the governing equations shown later for the motions of bubbles and molten Wood's-metal.

III. MATHEMATICAL MODEL FOR THE MOTIONS OF BUBBLES AND LIQUID

A. *Model Design*

Some mathematical models have been proposed to predict the mean bubble-rising velocity and mean liquid velocity in a bath agitated by isothermal gas injection.[17–23] Meanwhile, models capable of taking the heat transfer between the injected gas and the molten metal in the bath into consideration are very limited. In a previous study,[14] the authors proposed a simplified model for an isothermal gas injection system, too. Figure 1 shows a schematic of the flow field in the bath. The model will be extended here to consider the heat transfer between bubbles and liquid.

The heat exchange between cold bubbles and liquid in the bath was found to finish near the nozzle exit in the aforementioned three gas-liquid systems.[7] Accordingly, to predict the gas holdup (α), mean bubble-rising velocity, $\bar{u}_B$, and mean liquid velocity ($\bar{u}_L$), it is necessary to calculate a change in the temperature of a bubble rising in the region very close to the nozzle exit. For the prediction of the heat transfer between the bubble and the liquid, information on the mean bubble-rising velocity is required. In the presently proposed model, the mean liquid velocity is calculated from the equation of continuity for gas and the equations of motion for the gas and liquid. The slip model is used for the prediction of the mean bubble-rising velocity.[14]

$$\bar{u}_B = \bar{u}_L + \bar{u}_r \quad [9]$$

where $\bar{u}_r$ is the slip velocity.

In the following analysis, the gas holdup and the mean liquid velocity are assumed to follow Gaussian distributions:

$$\alpha = \alpha_{cl} \exp(-\ln 2 \cdot r^2/b_\alpha^2) \quad [10]$$

$$\bar{u}_L = \bar{u}_{L,cl} \exp(-\ln 2 \cdot r^2\lambda^2/b_\alpha^2) \quad [11]$$

$$\lambda = b_\alpha/b_u \quad [12]$$

where α_{cl} is the centerline value of gas holdup, b_α is the half-value radius of the gas holdup distribution, $\bar{u}_{L,cl}$ is the centerline value of the mean liquid velocity, r is the radial distance, b_u is the half-value radius of the mean liquid velocity distribution, and λ is the half-value radius ratio.

B. *Governing Equations*

The governing equations for gas and liquid in a bath agitated by gas injection are derived from previous articles.[14,22]

1. *Axial region in which $\alpha_{cl} \geq 0.5$*

The momentum of the injected gas is not fully transferred to the liquid in this axial region. According to Schneidesch *et al.*,[22] the following equations should be solved.

(1) Equation of continuity for gas

$$Q_{ga}H_a/(H_a + H_L - z)(\theta_g/\theta_{ge}) = \pi\alpha_{cl}b_\alpha^2 (\bar{u}_{L,cl}/2 + \bar{u}_r)/\ln 2 \quad [13]$$

where Q_{ga} is the volumetric gas flow rate evaluated at the atmospheric pressure, H_a is the height of a water column corresponding to the atmospheric pressure (*e.g.*, 10.3 m for 101.3 kPa), H_L is the bath depth, and z is the axial distance measured from the nozzle exit. It should be noted that the left-hand side of Eq. [13] is equal to the volumetric flow rate of gas in the bath, Q_g. The half-value radius ratio (λ) was assumed to be unity.

(2) Conservation of momenta of gas and liquid

The conservation of the momenta of gas and liquid is given by[22]

$$d/dz(\rho_L\pi\bar{u}_{L,cl}^2\, b_\alpha^2 (1 - 2\alpha_{cl}/3)/(2 \ln 2) + \rho_g\pi\alpha_{cl}\, b_\alpha^2 (\bar{u}_{L,cl}^2/3 + \bar{u}_{L,cl}\,\bar{u}_r + \bar{u}_r^2)/\ln 2) = 0.63\pi g(\rho_L - \rho_g)\, \alpha_{cl}\, b_\alpha^2/\ln 2 \quad [14]$$

where ρ_L is the density of liquid.

(3) Empirical equations for α_{cl} and b_α

The distributions of gas holdup, characterized by α_{cl} and b_α, which appear in the aforementioned governing equations, are calculated from empirical equations proposed previously by the authors.[23,24] The centerline value (α_{cl}) and the half-value radius of the gas holdup distribution (b_α) in this axial region are described as follows:

$$\alpha_{cl} = 0.5(0.9z/z_{50})^{-2n}/(1 + (0.9z/z_{50}{}^{-2n})^2)^{0.5} \quad [15]$$

where z_{50} is the axial position at which $\alpha_{cl} = 0.5$. The index n in Eq. [15] is given by

$$n = 0.027z_{50}/b_\alpha(z_{50}) + 0.38 \quad [16]$$

where $b_\alpha(z_{50})$ is the half-value radius of gas holdup at $z = z_{50}$. This value is selected because $z_{50}/b_\alpha(z_{50})$ falls between 0.09 and 0.385.[24]

The half-value radius is interpolated as

$$b_\alpha = b_{\alpha e} + (b_a\,(z_{50}) - b_{\alpha e})\,z/z_{50} \quad [17]$$

$$b_{\alpha e} = (\ln 2)^{0.5}\,d_{Be}/2 = 0.42d_{Be} \quad [18]$$

where $b_{\alpha e}$ is the half-value radius of the gas-holdup distribution at the nozzle exit. The bubble diameter at the nozzle exit (d_{Be}) is calculated from an empirical equation proposed by Mori and Sano.[25]

By referring to the previous experimental results for cold gas injection,[7,8] the half-value radius is expressed by[24]

$$b_\alpha\,(z_{50}) = c(Q_g{}^2/g)^{0.2}\,(\theta_L/\theta_{ge})^{0.2} \quad [19]$$

where the coefficient (c) is given by

$$c = 0.26(\rho_L/\rho_g)^{0,.07} \quad [20]$$

The axial distance, z_{50}, is known to be

$$z_{50} = ad_n\mathrm{Fr}_m{}^b \quad [21]$$

$$a = 0.77\,(\rho_L/\rho_g)^{0,.28} \quad [22]$$

$$b = 0.89\,(\rho_L/\rho_g)^{-0.16} \quad [23]$$

where d_n is the nozzle diameter and Fr_m is the modified Froude number, defined as

$$\mathrm{Fr}_m = \rho_g Q_g{}^2/(\rho_L g d_n{}^5) \quad [24]$$

In this analysis, the unknown parameters are $\bar{u}_{L,cl}$, $\bar{u}_r$, and θ_g. These quantities can be numerically calculated from Eqs. [5], [13], and [14] by referring to a previous article by the authors.[14]

2. *Axial region in which 0.1 ≤ α_{cl} < 0.5*

(1) Equation of continuity of gas

$$Q_{ga}H_a/(H_a + H - z)(\theta_g/\theta_{ge}) = \pi\alpha_{cl}b_\alpha{}^2\,(\bar{u}_{L,cl}/(1 + \lambda^2) + \bar{u}_r)/\ln 2 \quad [25]$$

where the half-value radius ratio, λ (equal to b_α/b_u), is assumed to be 0.65.[14]

(2) Conservation of momentum of liquid

According to the author's previous article,[14] the conservation of liquid is given by

$$d/dz\left(2\pi\int_0^\infty \rho_L\,(1 - \alpha)\bar{u}_L{}^2 r dr\right) = 2\pi\int_0^\infty g(\rho_L - \rho_g)\,\alpha r dr \quad [26]$$

Equation [26] can be rewritten as

$$\bar{u}_{L,cl}\,b_\alpha{}^2(1/(2\lambda^2) - \alpha_{cl}/(1 + 2\lambda^2)) = gb_\alpha{}^2\,(z_{50})z/2 + C \quad [27]$$

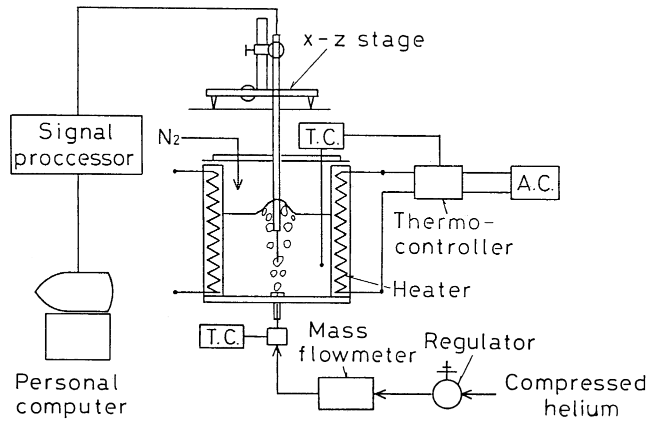

Fig. 2—Experimental apparatus.

The integration constant (C) can be given by substituting the values at $z = z_{50}$ into Eq. [27].

(3) Empirical equations for α_{cl} and b_α

The empirical equations for α_{cl} and b_α, described in a previous article by the authors,[23] are used in this regime.

$$\alpha_{cl} = 0.5\,(z/z_{50})^{-2n} \quad [28]$$

$$b_\alpha = b_\alpha\,(z_{50})\,(z/z_{50})^n \quad [29]$$

where the index n is calculated from Eq. [16].

3. *Axial region in which α_{cl} < 0.1*

The governing equations are the same as shown in a previous article by the authors,[14] and are not reproduced here. The following empirical equations are selected:[26]

$$\alpha_{cl} = 0.23\exp(-1.5z/z_5) \quad [30]$$

$$b_\alpha = 0.47b_\alpha\,(z_5)\exp(0.75\,z/z_5) \quad [31]$$

where z_5 is the axial distance at which $\alpha_{cl} = 0.05$.

$$z_5 = 17\,(Q_g{}^2/g)^{0.2} \quad [32]$$

$$b_\alpha(z_5) = 1.6(Q_g{}^2/g)^{0.2} \quad [33]$$

IV. EXPERIMENT

A. *Experimental Apparatus and Conditions*

Figure 2 shows a schematic of the experimental apparatus. The vessel diameter (D) and the height (H) were 200 and 300 mm, respectively. The bath depth (H_L) was 150 mm, and the liquid temperature (θ_L) was 378 K. The vessel selected in this study is a primary model for converters and ladles agitated by bottom-gas injection. The model vessel has a reduced scale of approximately one-tenth. The aspect ratio (H_L/D) was selected to be 0.75. The melting point of the molten Wood's-metal was 320 K. The flow rate of the compressed helium gas at 293 K was adjusted with a regulator and a mass-flow controller. The gas was cooled to 228 K and then injected through a single-hole bottom nozzle made of fluororesin into the molten Wood's-metal bath. The Wood's metal is an alloy of Sn, Pb, Cd, and Bi. The physical properties of the molten Wood's-metal and helium are listed

Table I. Physical Properties of Molten Wood's-Metal and Helium at 101 kPa

Fluid	Temperature (K)	Density (kg/m^3)	Kinematic Viscosity (mm^2/s)	Surface Tension (mN/m)
Wood's metal	378	9560	0.341	460
Helium	228	0.211	—	—
	378	0.129	183	—

in Table I. The volumetric flow rate at the nozzle exit (θ_{ge}) was 82.8 cm^3/s ($Q_{gN} = 90$ Ncm^3/s, where N indicates the normal condition). This gas injection condition is referred to as case C. The Wood's-metal temperature of 378 K (105 °C) was selected because it was suitable for obtaining reliable data with a magnet probe. The inlet temperature of helium was selected to increase the difference between the molten Wood's-metal temperature and the injected helium gas temperature as much as possible.

In a previous study,[27] the authors carried out model experiments on the bubble and liquid-flow characteristics in a molten steel bath agitated by isothermal gas injection. Molten Wood's metal and helium gas were selected as models for molten steel and argon. The main objective was to examine whether the results of the two characteristics obtained for a water-air system were useful to predict those in a molten metal bath. Accordingly, strict dimensionless-numbers matching was not given between the model and the actual process, although the model was considered as a primary model for converters and ladles. The present study was carried out by referring to Reference 27, and the same model fluids were selected. Wood's-metal was selected because the velocity measurements in it can be successfully carried out with a magnet probe. Helium was selected to simulate approximately the density ratio between molten steel and argon, although helium was not the most appropriate gas to simulate the gas injection in molten steel.

To clarify the effects of heat transfer on the two characteristics, measurements were carried out under two additional injection conditions.

(1) If the heat transfer between cold bubbles and liquid does not occur in the bath at all, the volumetric gas flow rate at the nozzle exit (Q_{ge}) is 82.8 cm^3/s, and the volumetric gas flow rate in the bath (Q_g) depends solely on the static pressure. This limiting situation was simulated by injecting helium gas of the same temperature as the molten Wood's-metal temperature of 378 K at Q_{ge} = 82.8 cm^3/s (referred to as case A).
(2) On the other hand, if the heat transfer between cold bubbles and liquid finishes completely at the nozzle exit, the volumetric gas flow rate at the nozzle exit becomes 131 cm^3/s. This limiting situation was simulated by injecting helium gas of 131 cm^3/s at 378 K (referred to as case B).

The three injection conditions can be summarized as follows:

case A: $Q_{ge} = 82.8$ cm^3/s, $Q_{gN} = 60N$ cm^3/s, $\theta_{ge} = \theta_L =$ 378 K (105 °C)

case B: $Q_{ge} = 131$ cm^3/s, $Q_{gN} = 90N$ cm^3/s, $\theta_{ge} = \theta_L =$ 378 K (105 °C)

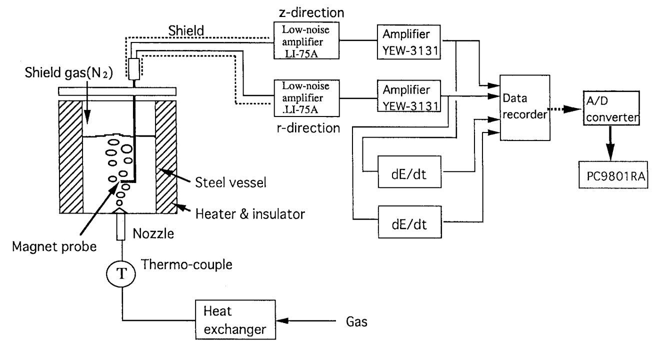

Fig. 3—Data acquisition and processing system.

case C: $Q_{ge} = 82.8$ cm^3/s, $Q_{gN} = 90N$ cm^3/s, $\theta_{ge} = 228$ K (−45 °C), $\theta_L = 378$ K (105 °C)

B. *Measurements of Gas and Liquid Temperatures*

The temperatures of bubbles and molten Wood's-metal in the axial region ranging from $z = 20$ to 80 mm were measured continuously with a alumel-chromel microthermocouple with a junction diameter of 12.5 μm. The details of its structure are described in a previous article.[7] The output signal of the thermocouple was A/D converted at a sampling frequency of 2.5 or 5 kHz and then processed on a personal computer to obtain the bubble temperature.

C. *Measurements of Bubble and Molten Wood's-Metal Flow Characteristics*

1. *Bubble characteristics*

The aforementioned experimental apparatus was also used to measure the bubble and liquid-flow characteristics in the molten Wood's-metal bath. The bath temperature was 378 K. A two-needle electroresistivity probe was used to measure the gas holdup and the mean bubble-rising velocity. The needle was made of enamel, and its diameter was 0.3 mm. It was coated with silicone except for its tip, for the sake of insulation. The output signal of the probe was A/D converted at a sampling frequency of 5 kHz and then processed on the personal computer to obtain the gas holdup and mean bubble-rising velocity.

2. *Velocity of molten Wood's-metal flow*

Although the details of the two-channel magnet probe measurements can be found in a previous article,[27] some important aspects will be reproduced here for a better understanding of the probe. Figure 3 shows the measurement system. The output signal was A/D converted at a sampling frequency of 200 Hz, and 2×10^4 pieces of data were stored on the computer. Discrimination of the signals originating from the bubbles and molten Wood's-metal was made by differentiating the output signal with respect to time. It is possible to simultaneously measure the axial and radial velocity components. Accordingly, the mean velocity components and the root-mean-square values of the turbulence components in the two directions, as well as the Reynolds shear stress, could be obtained. Only the mean velocity component in the axial direction will be presented in this article.

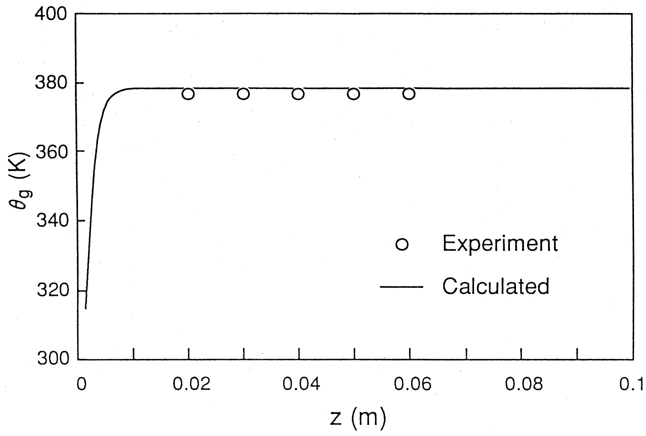

Fig. 4—Bubble temperature on the centerline of the bath.

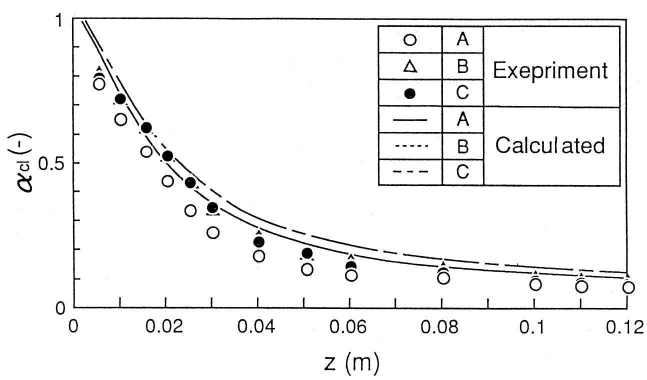

Fig. 5—Gas holdup on the centerline of the bath.

V. EXPERIMENTAL RESULTS AND DISCUSSION

A. *Bubble Temperature*

Figure 4 shows the numerically calculated and experimentally measured temperature distributions on the centerline of the bubbling jet. The measured values for $z \geq 20$ mm can be satisfactorily predicted by the mathematical model. It is evident that the calculated bubble temperature approaches the bath temperature of 378 K at around $z =$ 10 mm. This fact implies that the heat transfer between the bubbles and molten Wood's metal almost finishes just above the nozzle exit.

B. *Bubble Characteristics*

1. *Gas holdup*

Figure 5 shows the distributions of gas holdup on the centerline of the bubbling jet. The calculated results in cases B and C overlap each other, and, accordingly, the dotted line is not drawn in the figure. The measured values in cases B and C also nearly overlap each other. In each case, the measured values are slightly smaller than the calculated values. It can be concluded that the gas holdup on the centerline for the cold gas injection agrees with that for the isothermal gas injection of the same mass flow rate in the axial region considered. This fact also suggests that the heat transfer between bubbles and liquid finishes near the nozzle exit.

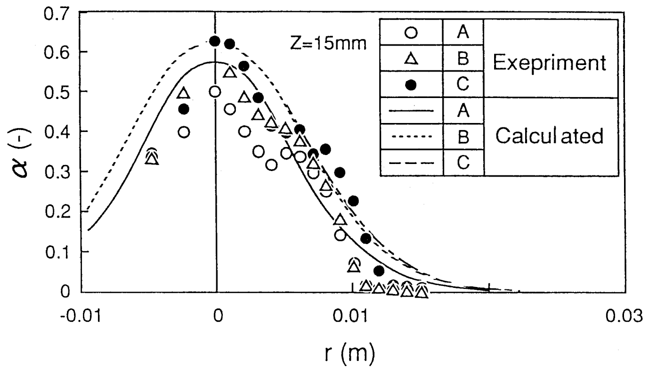

Fig. 6—Radial distributions of gas holdup at $z = 15$ mm (Eqs. [5], [13] and [14] were used to plot the calculated lines).

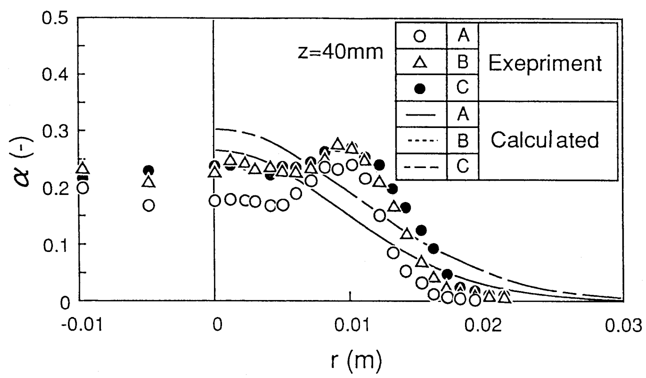

Fig. 7—Radial distributions of gas holdup at $z = 40$ mm (Eqs. [5], [25] and [27] were used to plot the calculated lines).

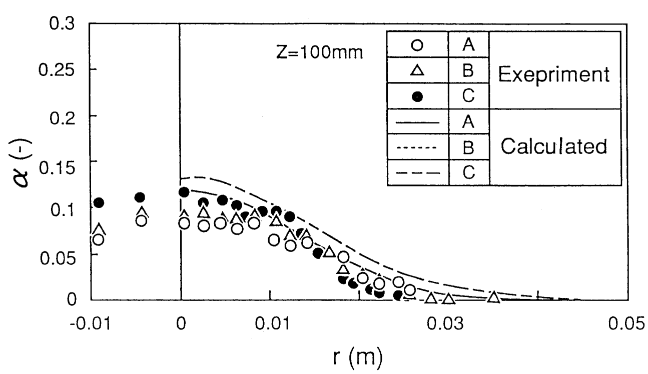

Fig. 8—Radial distributions of gas holdup at $z = 100$ mm (Eqs. [5], [25], and [27] were used to plot the calculated lines).

The radial distributions of gas holdup, measured at $z =$ 15, 40, and 100 mm, are shown in Figures 6 through 8, respectively. The distributions at $z = 40$ mm do not follow Gaussian distributions. This is because helium bubbles rising just above the nozzle exit are classified among the skirted bubbles, as mentioned in a previous article.[28] A representative result is reproduced in Figure 9. It is evident that the radial distribution of gas holdup at $z = 40$ mm typically reflects the shape of the bubble. The peak appearing at around $r = 10$ mm on the α distribution corresponds to the elongated part of the skirted bubble. The α distribution in case C is close to that in case B. As the axial distance

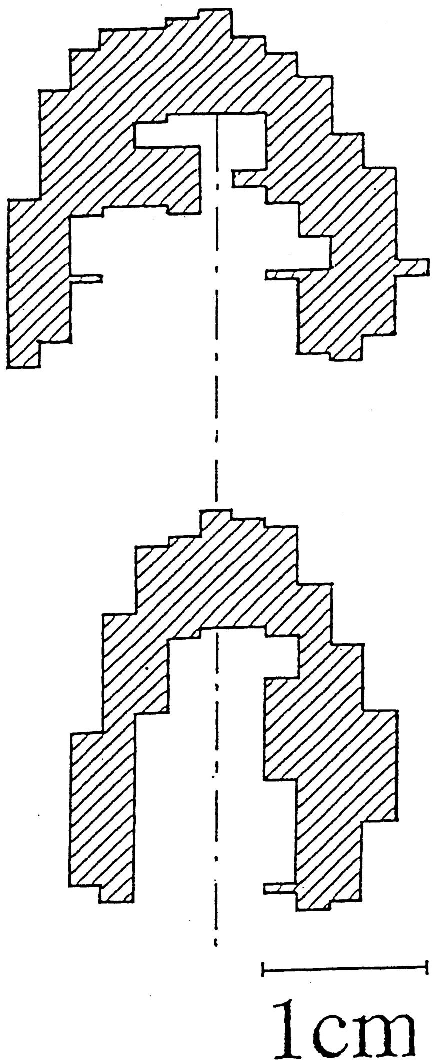

Fig. 9—Cross section of bubbles near the nozzle.

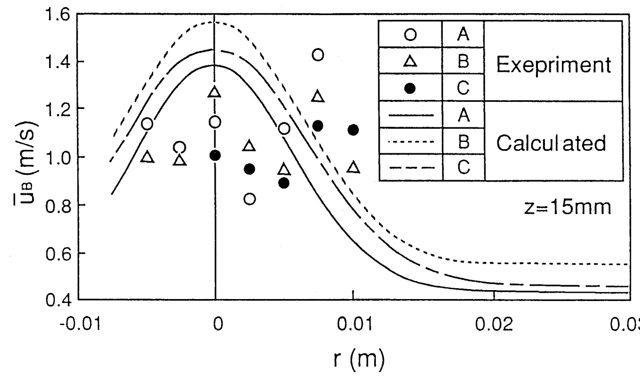

Fig. 10—Radial distributions of mean bubble rising velocity at z = 15 mm (Eqs. [5], [13], and [14] were used to plot the calculated lines).

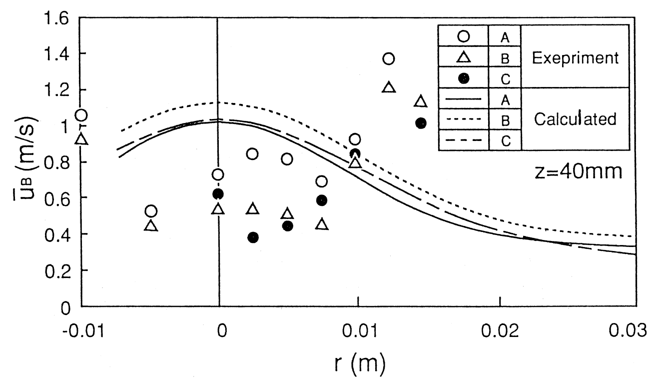

Fig. 11—Radial distributions of mean bubble rising velocity at z = 40 mm (Eqs. [5], [25], and [27], were used to plot the calculated lines).

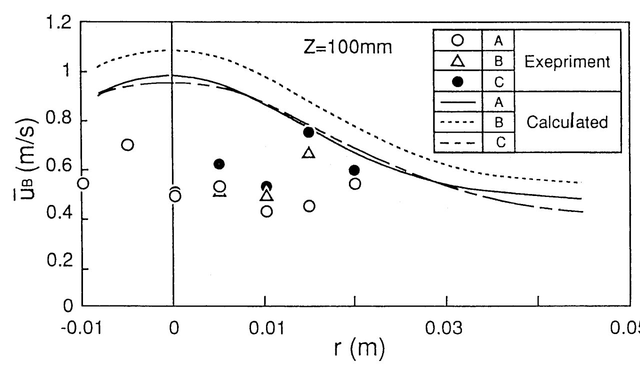

Fig. 12—Radial distributions of mean bubble rising velocity at z = 100 mm (Eqs. [5], [25], and [27] were used to plot the calculated lines).

increased, the skirted bubbles disintegrated into smaller bubbles due to strong turbulent shear stress caused by preceding bubbles. At z = 100 mm, the gas-holdup distributions for the three cases nearly follow Gaussian distributions, and they can be satisfactorily predicted by the presently proposed mathematical model. In the axial region above z = 100 mm, the model would be able to more satisfactorily predict the real distributions.

The measured value of α in case C is the largest among the three cases near the outer edge of the bubbling jet at z = 15 and 40 mm. The results mean that the injected cold gas expands farther in the radial direction than the isothermal gas injection. This behavior is consistent with the result obtained previously for cold gas injection into a water bath.[7]

2. *Mean bubble-rising velocity*

The radial distributions of the mean bubble-rising velocity, measured at z = 15, 40, and 100 mm, are shown in Figures 10 through 12, respectively. The measured distributions in the three cases (A, B, and C) do not satisfactorily agree with the calculated distributions at every z position. However, the measured values of $\overline{u}_B$ are scattered around the predicted curves, although the deviation is relatively large. Anyway, at present, it is difficult to accurately estimate the mean bubble-rising velocity near the nozzle exit. This situation is because the slip model was originally proposed not for the skirted bubbles, but for the wobbling bubbles. The measured values of $\overline{u}_B$ are high near the outer edge of the bubbling jet at z = 40 mm. Such distributions may be partly associated with the deformation of the skirted bubble.

As the distance from the nozzle exit increases, the skirted bubbles disintegrate into wobbling bubbles due to turbulence production in the wake of the bubbles. Under this condition, the previously proposed mathematical model would be useful for predicting the bubble-rising velocity.

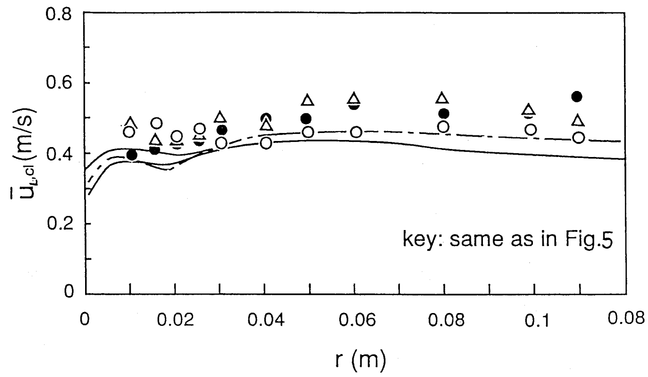

Fig. 13—Mean molten metal flow velocity on the centerline of the bath.

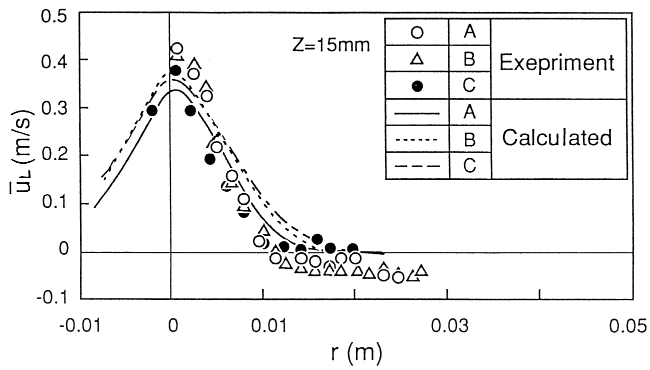

Fig. 14—Radial distributions of mean molten metal flow velocity at z = 15 mm (Eqs. [5], [13], and [14] were used to plot the calculated lines).

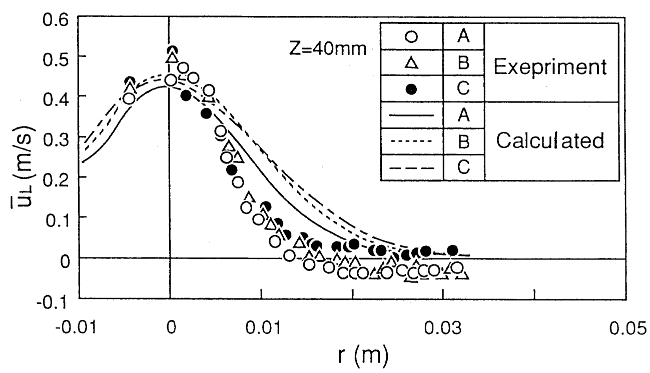

Fig. 15—Radial distributions of mean molten metal flow velocity at z = 40 mm (Eqs. [5], [25], and [27] were used to plot the calculated lines).

C. *Mean Velocity of Molten Wood's-Metal Flow*

Figure 13 shows the axial mean velocity of molten Wood's-metal flow on the centerline of the bubbling jet. The calculated value in case C approaches the calculated value in case B as z increases beyond z = 20 mm. The same is true for the measured values. The result obtained in this study can be explained by the fact that the injected cold gas expands completely to a value calculated from the bath temperature of 378 K and the static pressure just above the nozzle exit. The measured values in the three cases can be satisfactorily approximated by the calculated values.

Figures 14 through 16 show the radial distributions of the axial mean velocity components of molten Wood's-metal

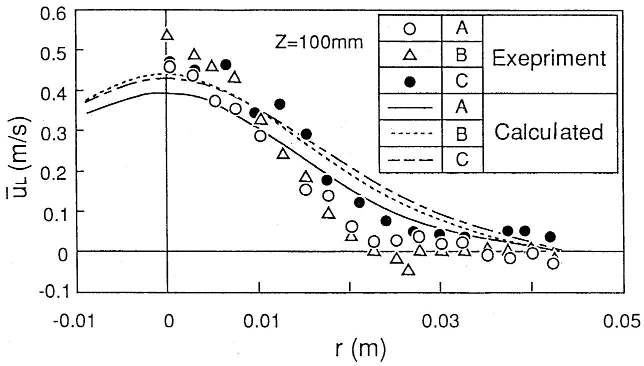

Fig. 16—Radial distributions of mean molten metal flow velocity at z = 100 mm (Eqs. [5], [25], and [27] were used to plot the calculated lines).

flow. At the axial positions of z = 15 and 40 mm, the measured values of $\bar{u}_L$ in case C are the largest near the outer edge of the bubbling jet. This result is consistent with the radial distribution of gas holdup, shown in Figures 6 and 7. The measured values of $\bar{u}_L$ can be satisfactorily approximated by the present model. It is interesting to note that the radial distribution of the mean velocity of molten Wood's-metal flow is close to the Gaussian distribution, although the radial distribution of gas holdup is different from that distribution. Hetsroni[29] found that the wake behind a bubble becomes turbulent for a bubble Reynolds number (Re_B) greater than approximately 400. Such additional turbulence production is the main cause for the Gaussian-like distributions of the mean molten Wood's-metal flow velocity.

VI. CONCLUSIONS

This study is concerned with the role of heat transfer between bubbles and liquid on the behavior of bubbles and liquid-flow velocity in a molten Wood's-metal bath agitated by cold helium gas injection. The main findings obtained in this study can be summarized as follows.

1. Under the experimental conditions considered, bubbles were successively generated at the nozzle exit. The heat transfer between the cold bubbles and molten Wood's-metal finished near the nozzle exit. As a result, the axial distribution of gas holdup on the centerline of the bubbling jet came to agree with that for an isothermal gas injection of the same mass flow rate as the axial distance increased.
2. The radial distribution of gas holdup measured near the nozzle exit was closely associated with the shape of the bubbles. As the bubbles disintegrated into smaller bubbles with a further increase in the axial distance, the distribution approached a Gaussian distribution. The measured radial distribution of gas holdup came to be approximated by a mathematical model proposed in this study as the axial distance increased.
3. The prediction of the radial distribution of the mean bubble-rising velocity is not satisfactory. The measured values of $\bar{u}_B$, however, are scattered around the predicted curve, although the deviation is relatively large.
4. The measured distribution of the mean molten Wood's-metal flow velocity on the centerline of the bubbling

jet for cold gas injection came to follow the measured distribution for the isothermal gas injection of the same mass flow rate as *z* increased.

5. The measured radial distribution of the mean molten Wood's-metal flow velocity also approached a Gaussian distribution as the axial distance increased. This behavior is because the skirted bubbles generated at the nozzle exit disintegrated into smaller bubbles like the wobbling bubbles due to strong turbulent mixing. The measured distribution came to be approximated by the presently proposed mathematical model.

REFERENCES

1. J. Szekely, G., Carlsson, and L. Helle: *Ladle Metallurgy*, Springer-Verlag, New York, NY, 1989.
2. Y. Sahai and G.R. St. Pierre: *Advances in Transport Processes in Metallurgical Systems*, Elsevier, Amsterdam, 1992.
3. D. Mazumdar and R.I.L. Guthrie: *Iron Steel Inst. Jpn. Int.*, 1995, vol. 35 (1), pp. 1-20.
4. *Recent Development in Steelmaking Technologies Using Gas Injection*, Proc. 100th and 101st Nishiyama Memorial Lecture, ISIJ, 1984.
5. H. Kajioka: *Ladle Refining*, Chijin Book Co. Ltd., Tokyo, 1997.
6. O.J. Ilegbusi, M. Iguchi, and W. Wahnsiedler: *Mathematical and Physical Modeling of Materials Processing Operations*, Chapman & Hall/CRC, Boca Raton, FL, 1999.
7. M. Iguchi, Z. Morita, H. Tokunaga, and H. Tatemichi: *Iron Steel Inst. Jpn. Int.*, 1992, vol. 32 (7), pp. 865-72.
8. H. Tokunaga, M. Iguchi, and H. Tatemichi: *Iron Steel Inst. Jpn. Int.*, 1995, vol. 35 (1), pp. 21-5.
9. M. Iguchi, S. Kodani, and H. Tokunaga: *Steel Res.*, 2000, vol. 71 (11), pp. 435-41.
10. S.V. Komarov and M. Sano: *Iron Steel Inst. Jpn. Int.*, 1998, vol. 38 (10), pp. 1045-52.
11. M. Iguchi, H. Kawabata, K. Nakajima, and Z. Morita: *Metall. Mater. Trans. B*, 1995, vol. 26B, pp. 67-74.
12. R. Ricou and C. Vives: *Int. J. Heat Mass Transfer*, 1982, vol. 25 (2), pp. 1579-88.
13. T. Weissenfluh: *Int. J. Heat Mass Transfer*, 1985, vol. 28, pp. 1563-74.
14. M. Iguchi, Z. Morita, H. Tokunaga, H. Tatemichi, Y. Sakamoto, and S. Takagi: *Tetsu-to-Hagané*, 1993, vol. 79 (5), pp. 25-32.
15. R.B. Bird, W.E. Stewart, and E.N. Lightfoot: *Transport Phenomena*, John Wiley & Sons, New York, NY, 1996.
16. H. Uchida: *Heat Transfer*, Shokabo Book Co. Ltd., Tokyo 1983, p. 343.
17. M. Sano and K. Mori: *Tetsu-to-Hagané*, 1982, vol. 68, p. 2451.
18. S. Asai, T. Okamoto, J.-C. He, and I. Muchi: *Tetsu-to-Hagané*, 1982, vol. 68, pp. 426-34.
19. J.-C. He and S. Asai: *Tetsu-to-Hagané*, 1984, vol. 70, pp. 1590-97.
20. N.A. Hussain and R. Siegel: *Trans. ASME, J. Fluids Eng.*, 1976, vol. 101, p. 49.
21. Y. Xie and F. Oeters: *Steel Res.* 1992, vol. 63 (3), p. 93.
22. C.R. Schneidesch, H.J. Richter, and P.E. Queneau: *The Reinhardt Schuhmann Int. Symp. on Innovative Technology and Reactor Design in Extraction Metallurgy*, D.R. Gaskel *et al.*, eds., TMS, Warrendale, PA, 1986, p. 43.
23. M. Iguchi, K. Nozawa, and Z. Morita: *Iron Steel Inst. Jpn. Int.*, 1991, vol. 31, pp. 952-59.
24. M. Iguchi, Y. Demoto, N. Sugawara, and Z. Morita: *Iron Steel Inst. Jpn. Int.*, 1992, vol. 32, pp. 998-1005.
25. K. Mori and M. Sano: *Tetsu-to-Hagané*, 1981, vol. 67 (6), pp. 672-95.
26. M. Iguchi, K. Nozawa, H. Tomida, and Z. Morita: *Iron Steel Inst. Jpn. Int.*, 1992, vol. 32, pp. 747-53.
27. M. Iguchi, H. Tokunaga, and H. Tatemichi: *Metall. Mater. Trans. B*, 1997, vol. 28B, pp. 1053-61.
28. M. Iguchi, K. Nakatani, and H. Tokunaga: *Metall. Mater. Trans. B*, vol. 28B, 1997, pp. 417-23.
29. G. Hetsroni: *Int. J. Multiphase Flow*, 1989, vol. 15, pp. 735-46.